Chemical Science

EDGE ARTICLE

View Article Online
View Journal | View Issue



Cite this: *Chem. Sci.*, 2018, **9**, 5736

# Mechanistic insights into the $S_N2$-type reactivity of aryl-Co(III) masked-carbenes for C–C bond forming transformations†

O. Planas, ‡ [a] S. Roldán-Gómez, ‡[a] V. Martin-Diaconescu, [b] J. M. Luis, *[a] A. Company [a] and X. Ribas *[a]

Received 21st February 2018
Accepted 28th May 2018

DOI: 10.1039/c8sc00851e

rsc.li/chemical-science

Herein we describe the synthesis and characterization of a family of C-metalated aryl-Co(III) enolates, which can be considered as masked-carbenes, using diazoacetates as coupling partners. These species have been proved to be necessary intermediates in the $C(sp^2)–C(sp^3)$ bond forming event to obtain cyclic amides, taming the elusive Co(III)-carbene species. The scope of diazoacetates has been exhaustively examined, varying the nature of the ester and the α-substitution, and a clear preference for electron-poor carbene precursors is observed. Exhaustive experimental and theoretical studies indicate that an unprecedented intramolecular $S_N2$-type process governs the formation of the newly formed C–C bond. Furthermore, the key role of several Lewis acids as carboxylate-activating reagents is further explored by DFT calculations.



## Introduction

Recently, transition-metal-catalyzed C–H bond activation has emerged as a powerful and versatile tool in organic synthesis.[1–3] Most of the achievements have been accomplished with precious metals such as Rh, Ru and Pd.[4–10] However, methodologies using more abundant and cost-efficient 3d transition metal catalysts have attracted increasing attention in the field of directed C–H activation and functionalization.[11–14] Indeed, this recent interest in first-row transition metal catalysts has allowed the development of new C–H functionalization protocols for the synthesis of several organic molecules using Fe,[15–17] Mn[18,19] and Ni[20,21] as catalysts. Particularly, Co has attracted recent interest probably due to the practicality and efficiency of group 9 metals. Two different approaches coexist in the field of Co-catalyzed C–H functionalization: the low-valent approach,[22,23] which has been extensively studied, and the high-valent approach.[24]

The high-valent approach in Co-catalysis has emerged as a tremendously valuable tool for the construction of organic scaffolds through the use of Cp*Co(III) catalysts[25–27] as well as *N*′*N*-bidentate-chelating directing groups.[28] Knowledge of the mechanistic pathways governing these transformations is still in its infancy,[29] although an organometallic Co(III) species is generally implicated.[30,31] Proof-of-concept protocols reported by Broderick and Legg[32,33] and Avilés[34] provided early evidence of organometallic Co(III) species obtained through C–H activation. After these two examples the field remained dormant until recently, when several cobaltacycles synthesized through C–H activation were reported.[30,31,35] Indeed, cobalt has recently been proved to be a practical metal to perform a vast array of transformations. Particularly, the use of carbene precursors has attracted recent interest due to their versatility as coupling partners in transformations such as carbonylation[36,37] and annulation,[38–44] including Co(III)-radical-based outer-sphere functionalization (Scheme 1a). Regarding C–H functionalization, the field was pioneered by Miura using Co(II) salts.[45] Recently, the use of Cp*Co(III) catalysts allowed several organometallic C–H functionalization reactions utilizing diazo esters as coupling partners (Scheme 1b).[46–50] The reactivity observed with Co(III) is currently rationalized through the formation of an elusive aryl-Co(III)-carbene (**B**, Scheme 1c), which undergoes migratory insertion to furnish the corresponding alkyl-Co(III) intermediate (**C**, Scheme 1c).[51] This rationalization is indeed not surprising, thus migratory insertion into metal–carbon bonds is a common pathway in metal–carbene functionalization reactions.[52]

The mechanistic understanding of metal-catalyzed transformations constitutes a landmark of our research.[53–56] To achieve this goal, a variety of macrocyclic model substrates can be utilized, as they proved to be key for the synthesis and characterization of several organometallic intermediates.[57–59] Following this line, we have recently published the synthesis and characterization of a family of aryl-Co(III) complexes through C–H activation.[60] These complexes were competent

[a]*Institut de Química Computacional i Catàlisi (IQCC), Departament de Química, Universitat de Girona, Campus Montilivi, Girona, E-17003, Catalonia, Spain. E-mail: josepm.luis@udg.edu; xavi.ribas@udg.edu*

[b]*Institute of Chemical Research of Catalonia (ICIQ), The Barcelona Institute of Science and Technology, Avinguda Països Catalans 16, 43007 Tarragona, Catalonia, Spain*

† Electronic supplementary information (ESI) available: CCDC 1825084 (**4a-OPiv**), 1825085 (**4a-OBz**), 1825086 (**4a-OBz-NO$_2$**), and 1825087 (**4a-OBz-COMe**) contain the supplementary crystallographic data for this paper. For ESI and crystallographic data in CIF or other electronic format see DOI: 10.1039/c8sc00851e

‡ Equally contributing author.

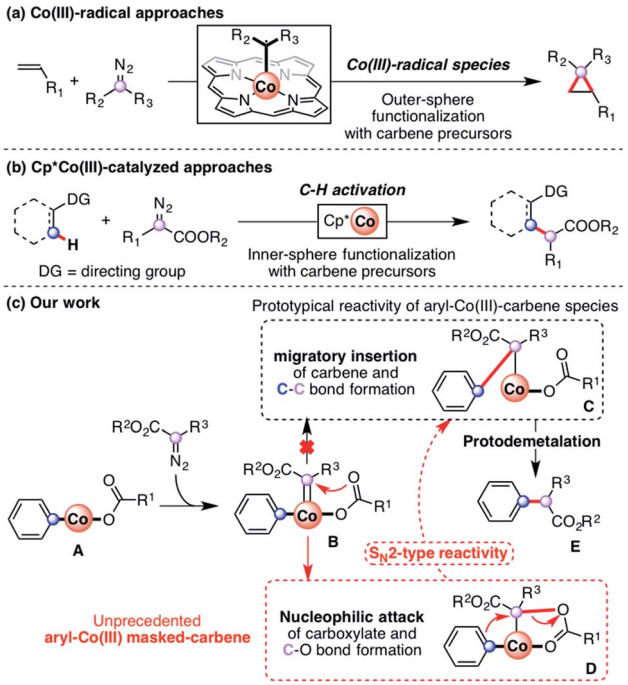


Scheme 1 Reactivity of Co(III) species with diazoacetates: (a) functionalization through Co(III)-radical species; (b) C–H activation utilizing Cp*Co(III) catalysts; (c) prototypical migratory insertion mechanism (black) and our work, which proved the existence of new intermediates using macrocyclic model substrates (red).

intermediates during alkyne annulation reactions, as well as diazoacetate couplings.[61] When our aryl-Co(III) complexes reacted with ethyl diazoacetate (EDA) under anhydrous conditions, an unprecedented C-metalated aryl-Co(III) enolate was obtained (**D**, Scheme 1c). Thus, the nucleophilic attack of the adjacent carboxylate moiety gives a rare *cis* aryl-Co(III)-alkyl organometallic species, which was never considered until our report and constitutes a unique example in the field. Interestingly, this intermediate **D**, which can be considered either as a masked-carbene moiety or a carbenoid, evolves to intermediate **C** (Scheme 1c) through a rare intramolecular S$_N$2-type pathway in which the carboxylate moiety acts as both a relay and a leaving group. Then, after protodemetalation of **C** the corresponding organic product containing a new C–C bond (**E**, Scheme 1c) can be released and the Co(III) catalyst is regenerated.

Herein we report on the full understanding of the electronic and steric effects that control this carbene transfer *via* the masked-carbene strategy. To that end, the synthesis of a family of C-metalated aryl-Co(III) enolates bearing differently substituted carboxylate moieties (R$^1$, Scheme 2), using a macrocyclic ligand as a model substrate, is reported. Moreover, several diazoacetates bearing substituents with different electronic and steric properties will be tested (R$^2$ and R$^3$, Scheme 2). Finally, new pieces of experimental and computational evidence are reported to provide a broader mechanistic insight into the formation of aryl-Co(III) masked-carbenes as well as into the unique intramolecular S$_N$2-type reactivity to obtain new C–C bonds.

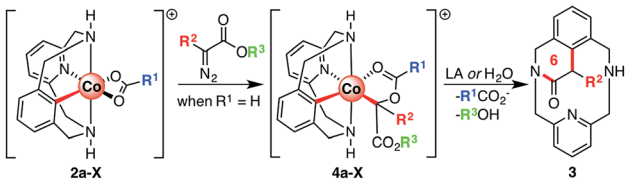


Scheme 2 Reactivity of aryl-Co(III) bearing different carboxylate ligands (R$^1$) with diazoacetates with diverse substituents on the α-(R$^2$) and ester (R$^3$) positions.

## Results and discussion

Initially, several organometallic aryl-Co(III) intermediates bearing different carboxylate anions (**2a-X**, X = TFA, TPA (triphenylacetate), OPiv, or OBz-Y; Y = H, Me, OMe, Cl, COMe, CN, or NO$_2$) were synthesized starting from **1a-H**, CoBr$_2$ and the corresponding silver carboxylate salts (see the ESI† for more details). Then, **2a-X** were tested in the annulation reaction utilizing ethyl diazoacetate (EDA) as a coupling partner to furnish the cyclic amide **3a** (Scheme 3). First, following our previous work,[61] aryl-Co(III) species bearing alkyl carboxylates were tested using 2.0 equiv. of EDA and 4.0 equiv. of H$_2$O as additives in 2,2,2-trifluoroethanol (TFE) at 100 °C (alkyl, Scheme 3). We recently reported that the reaction of **2a-OAc** and **2a-TFA** with EDA furnished **3a** in excellent yields. To further understand this transformation, we attempted the reaction of EDA with sterically crowded aryl-Co(III) carboxylates such as **2a-OPiv** and **2a-TPA**. Interestingly, when R$^1$ = $^t$Bu (OPiv), **3a** was furnished in poor yield (20–23%), even in the presence of Lewis acids such as LiOTf. This result suggests that carboxylates bearing bulky groups inhibit the reaction. Indeed, when **2a-TPA** was reacted with EDA, **3a** was obtained in trace amounts. It should be noted that triphenylacetate is a weak base and subsequently, a good leaving group. However, the bulky "CPh$_3$" moiety inhibits the formation of **3a**, indicating that steric effects play an important role too. The formation of cyclic amide **3a** was also studied starting from aryl-Co(III) complexes bearing differently *p*-substituted benzoate anions (**2a-OBz-Y**; Scheme 3). In

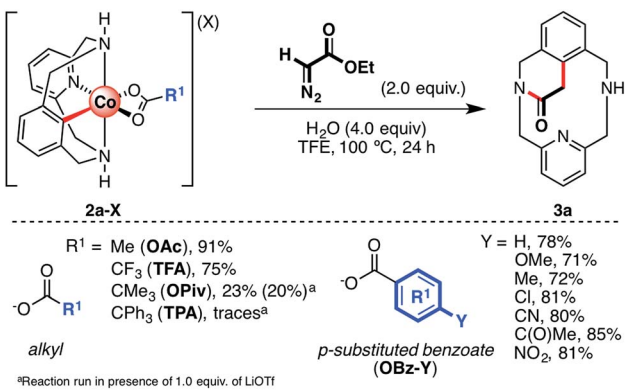


Scheme 3 Reaction scope with a variety of alkyl and *p*-substituted aryl carboxylate ligands. Yields were determined after isolation by silica column chromatography.

this case, when 4.0 equiv. of $H_2O$ were added, **3a** was obtained in good yields (71–85%) regardless of the substitution of the carboxylate moiety. Thus, the electronic properties of the carboxylate anions have little impact on the yield of **3a** under these particular reaction conditions.

Reactivity of **2a-OAc** with a variety of substituted diazoesters was also evaluated (Scheme 4) in the presence of 4.0 equiv. of $H_2O$ and TFE as the solvent. First, we evaluated the substitution on the ester moiety using a variety of alkyl and aryl diazoacetates ($R^3$, Scheme 4). When the ester moiety bears an alkyl fragment such as a methyl, ethyl, *tert*-butyl, benzyl or aryl moiety, the reaction proceeds with good to excellent yields, affording macrocyclic amide **3a**. In spite of the promising reactivity with EDA, no product was observed when **2a-OAc** was reacted with a variety of α-substituted ethyl diazocarboxylate moieties ($R^2$, Scheme 4), in contrast to the described reactivity of Cp*Co(III) catalysts.[46–51] Indeed, when a methyl (**b**) or a benzyl (**c**) moiety was present in the α-position, only traces of **3b** or **3c** were detected. Surprisingly, when ethyl diazomalonate (**d**) was used as a coupling partner, the unexpected formation of **3a** was observed in 73% yield after decarboxylation. Thus, only acceptor/acceptor carbene precursors engage in coordination and annulation to furnish product **3**. However, trace amounts of products were detected when a highly electron-withdrawing group (trifluoromethyl (**e**), nitro (**f**) and cyano (**g**) groups) was directly attached in the α-position with respect to the diazo carbon, probably due to its high reactivity. Furthermore, when electron-rich aryl moieties such as phenyl (**h**) and *p*-OMe-phenyl (**i**) are attached to the α-position of ethyl diazoacetate, trace amounts of the corresponding cyclic amides **3h** and **3i** are obtained. However, if the phenyl group contains an electron-withdrawing group, such as a bromide (**j**), trifluoromethyl (**k**) or nitro (**l**) group, the corresponding amides **3j**, **3k** and **3l** are obtained in good yields (65–74%) in the presence of 1.0 equiv. of LiOTf as additive. These results suggest that the formation of aryl-Co(III)-carbenes and their subsequent reactivity depends on both steric and electronic properties of the diazoacetate. Thus, in contrast to the previously reported methodologies,[46–51] the reaction with acceptor/donor diazoacetates does not proceed while acceptor/acceptor carbene precursors afford amide **3**.

In order to further compare the reactivity of different substrates under the optimized reaction conditions, we performed several intermolecular competition reactions (Scheme 5). First, the electronic properties of the carbene precursor were tested through a reaction of **2a-OAc** and 4.0 equiv. of ethyl *p*-substituted-phenyl diazoacetates **j** and **l** (Scheme 5a) in the presence of 4.0 equiv. of $H_2O$ and 1.0 equiv. of LiOTf as additives. Under these conditions, **3j** was obtained in 47% yield while **3l** was furnished in 32% yield (79% combined isolated yield). Thus, both electron-poor carbene precursors **j** and **l** react similarly with **2a-OAc** (ratio 1.5 : 1). Thereafter, the steric effects of the diazoacetate coupling partners were evaluated through an intermolecular competition

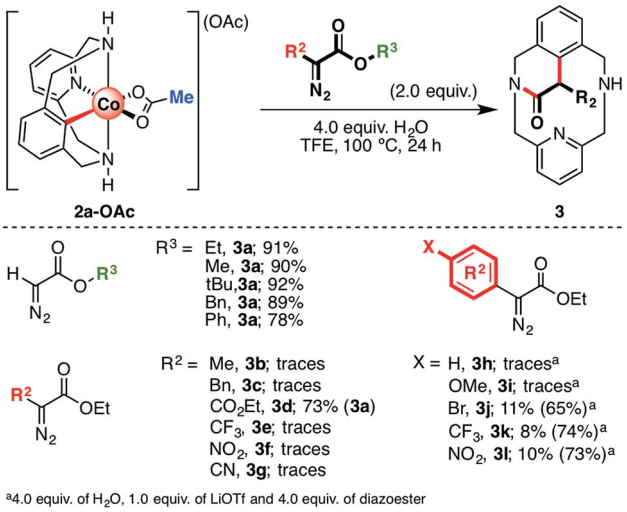


Scheme 4 Reaction scope with several ester-substituted ($R^3$) and α-substituted ($R^2$) diazo compounds. Yields were determined after isolation by silica column chromatography.

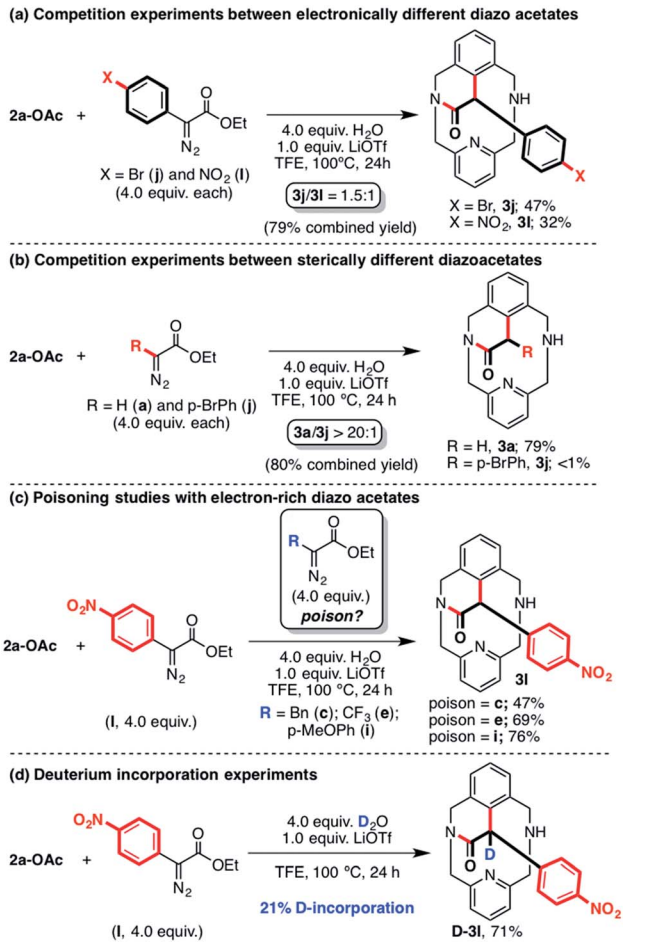


Scheme 5 (a) Competition experiments using diazo esters with different electronic properties. (b) Competition experiments using diazo esters with different steric properties. (c) Poisoning studies of the reaction between **2a-OAc** and diazo acetate **l**, using diazoacetates **c**, **e** and **i** as potential poisons. (d) Deuterium incorporation into **3l** using labeled water as the additive. Isolated yields after silica column chromatography; ratios determined by proton NMR.

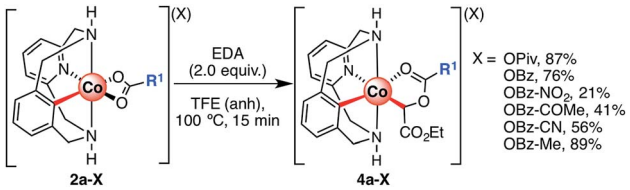


Scheme 6 Synthesis of C-metalated aryl-Co(III) enolates bearing a variety of carboxylate anions (**4a-X**, where X = carboxylate anion). Yields after recrystallization.

experiment between diazo esters **a** and **j** (Scheme 5b). When 4.0 equiv. of each carbene precursor were mixed with **2a-OAc** in TFE, exclusive formation of **3a** was observed (ratio **3a**/**3j** > 20 : 1). Thus, this result indicates that the reaction of **2a-OAc** with sterically demanding carbene precursors is not favored in the presence of EDA, subsequently forming cyclic amide **3a** as a single product. Finally, as the reaction of **2a-OAc** with some precursors was not successful, diazo esters **c**, **e** and **i** were tested as poisoning reagents (Scheme 5c) in the reaction with diazo ester **l**. Under these conditions, the reaction yielded 47–76% of cyclic amide product **3l**, which clearly indicates that neither the alkyl-substituted diazoacetates (**c** and **e**) nor the electron-rich carbene precursor (**i**) inhibited the reactivity through either coordination or decomposition of the organometallic **2a-OAc** complex.

Deuterium labeling experiments were also performed using diazo ester **l** as a coupling partner in order to complement the examples that we previously reported (Scheme 5d).[61] It was found that when the reaction of **2a-OAc** with 4.0 equiv. of **l** was carried out using 4.0 equiv. of $D_2O$ as the additive instead of ordinary water, **3l** was obtained in 71% yield and a 21% D-incorporation was observed by $^1H$ NMR analysis (see Fig. S1†). This result is in agreement with the previously reported D-labeling experiments, indicating a possible proto-demetalation step prior to the formation of the corresponding cyclic amide **3**.

To gain further insight into the reaction mechanism, several C-metalated aryl-Co(III) enolate complexes bearing a variety of carboxylate ligands (**4a-X**) were synthesized (Scheme 6). When **2a-X** was reacted with 2.0 equiv. of EDA at 100 °C for 15 minutes, the corresponding **4a-X** intermediates were obtained in moderate to excellent yields (21–89%). Characterization by NMR and HRMS indicated the formation of diamagnetic aryl-Co(III) species bearing an alkyl moiety corresponding to the EDA fragment. Indeed, the structure of intermediates **4a-X** was further confirmed by XRD analysis (Fig. 1; X = OPiv (a), OBz (b), OBz-$NO_2$ (c) and OBz-COMe (d)). The solid-state structures of **4a-X** showed the formation of an $O_h$ aryl-Co(III) center bearing a carbonyl group *trans* to the aryl moiety. In the *cis*-position with respect to the aryl fragment, a C-enolate binds to the metal center as an alkyl ligand (**4a-OPiv**; Co–C1 = 1.962 Å), thus providing an unusually stable *cis*-aryl-Co(III)-alkyl organometallic intermediate. Overall, the solid-state structures present similar XRD features and show the formation of rare C-metalated aryl-Co(III) enolates, which are presumably formed through a nucleophilic attack of the carboxylate anion to a putative highly electrophilic Co(III)-carbene. Remarkably, it should be noted that the C2–O2 distance is slightly larger with electron-poor benzoate moieties (**4a-OBz**, C2–O2 = 1.480 Å; **4a-OBz-NO$_2$**, C2–O2 = 1.507 Å), which indicates that species bearing electron-poor fragments might be more prone to evolve to amide **3** through an intramolecular $S_N2$-like mechanism.

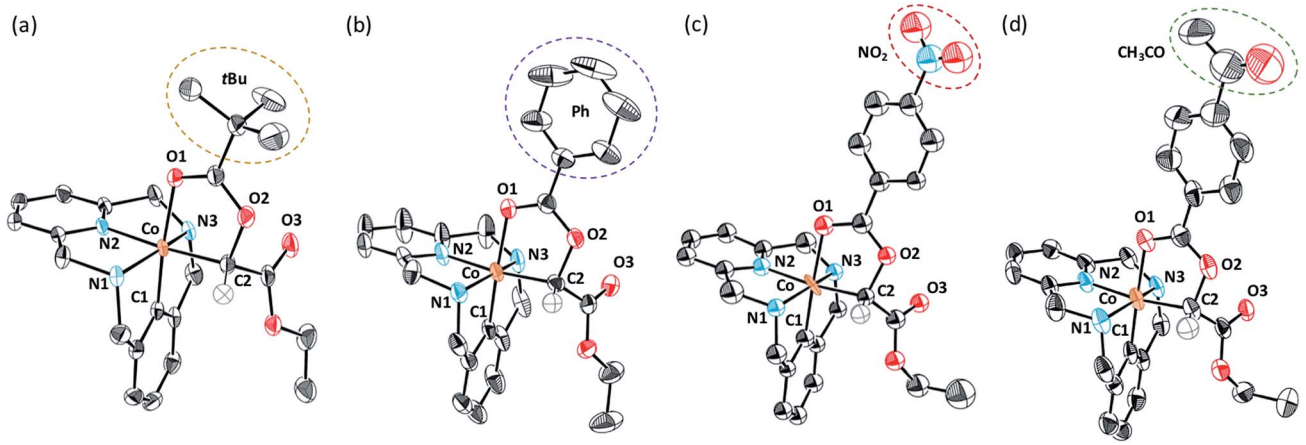


Fig. 1 Solid state structures of organometallic aryl-Co(III)-alkyl compounds **4a-X**. Hydrogen atoms, carboxylate anions and solvent molecules have been omitted for clarity; only one of the enantiomers is depicted; ellipsoids are set at 50% probability. (a) Crystal data for **4a-OPiv**. Selected bond distances [Å] and angles [°]: Co–C(1) 1.840(6), Co–C2 1.962(4), Co–N(1) 2.002(4), Co–N(2) 1.892(3), Co–N(3) 1.994(4), Co–O(1) 2.023(4), C(2)–O(2) 1.480(7); C(1)–Co–C(2) 92.7(2), C(1)–Co–O(1) 174.8(2). (b) Crystal data for **4a-OBz**. Selected bond distances [Å] and angles [°]: Co–C(1) 1.853(2), Co–C2 1.971(4), Co–N(1) 2.003(4), Co–N(2) 1.893(3), Co–N(3) 2.008(4), Co–O(1) 1.989(4), C(2)–O(2) 1.480(7); C(1)–Co–C(2) 95.5(2), C(1)–Co–O(1) 177.4(2). (c) Crystal data for **4a-OBz-NO$_2$**. Selected bond distances [Å] and angles [°]: Co–C(1) 1.809(2), Co–C2 1.976(4), Co–N(1) 2.002(4), Co–N(2) 1.899(3), Co–N(3) 1.981(4), Co–O(1) 2.000(4), C(2)–O(2) 1.507(7); C(1)–Co–C(2) 94.1(1), C(1)–Co–O(1) 175.3(2). (d) Crystal data for **4a-OBz-COMe**. Selected bond distances [Å] and angles [°]: Co–C(1) 1.849(2), Co–C2 1.978(4), Co–N(1) 2.002(4), Co–N(2) 1.886(3), Co–N(3) 2.000(4), Co–O(1) 2.016(4), C(2)–O(2) 1.499 (7); C(1)–Co–C(2) 95.8(1), C(1)–Co–O(1) 177.9(2).

Once the organometallic **4a-X** complexes were analyzed and characterized, we evaluated their capability to evolve to product **3a** through an intramolecular $S_N2$-type mechanism. Firstly, **4a-OBz-Y** complexes were heated at 100 °C for 24 h utilizing TFE as the solvent. Interestingly, **3a** was observed regardless of the electronic properties of the *para*-substituted benzoate ester, albeit higher yields were obtained with electron-withdrawing substituents (see Table S1†). The evolution of **4a-OBz-Y** was further studied by means of kinetic analysis. Electronic effects on the C–C bond formation were tested through a Hammett plot prepared following Chatani's method,[62,63] in which the evolution of an electronically different set of *para*-substituted benzoate species (**4a-OBz-Y**) to cyclic amide **3a** was compared at short reaction times (Fig. 2). Thus, **4a-OBz-Y** were heated in anhydrous TFE over 3 h and the crude mixture was analyzed by proton NMR using 1,3,5-trimethoxybenzene as the internal standard (Fig. 2a). Then, the amount of **3a** obtained starting from **4a-OBz-Y** ($\mathbf{Y_Y}$) was compared to the yield obtained from **4a-OBz-H** ($\mathbf{Y_H}$). A linear correlation ($R^2 = 0.963$) from the conversion of the corresponding organometallic complexes *vs.* the Hammett parameter ($\sigma_p$) led to a positive slope value of $\rho = 0.568$. This value is consistent with a rate-determining step, the transition state of which builds partial negative charge (Scheme 5). Further evidence of an $S_N2$-type mechanism was obtained when product yields were correlated with the acidity of the leaving group (LG) conjugate acid in a Brønsted plot. As shown in Fig. 2b, a linear correlation ($R^2 = 0.963$) was obtained, leading to a negative value of $\beta_{LG} = -0.573$. Thus, in spite of the moderate value obtained ($0 > \beta_{LG} > -1$), this result clearly indicates that the leaving group ability plays a role in the rate-determining step of this transformation.[64] However, **2a-TPA**, whose corresponding enolate corresponds to a good leaving group ($pK_a$(TPAH) = 3.33), is found to be unreactive towards the formation of **3a**. This result suggests that steric factors have to be taken into account too. In addition to these experiments, a surprisingly good linear correlation ($R^2 = 0.973$) between the $^{13}C$ chemical shift of the C-enolate moiety (C2, Fig. 2c) and the corresponding Hammett parameter of **4a-OBz-Y** complexes was found. Indeed, the plot in Fig. 2c suggests that the electronic properties of the substituent have a considerable effect on the

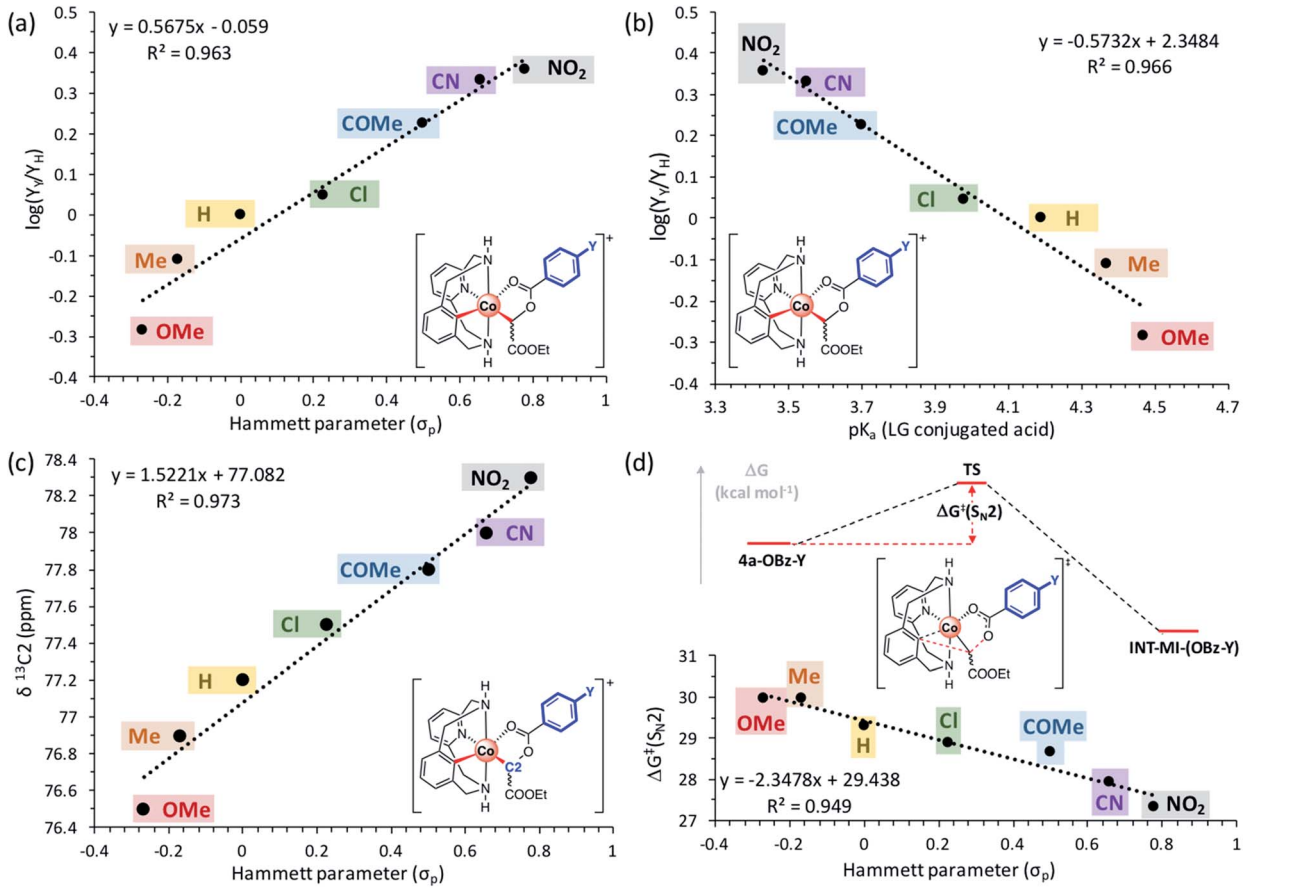


Fig. 2 (a) Hammett plot ($R^2 = 0.963$) of *para*-substituted benzoate C-metalated aryl-Co(III) enolate complexes (**4a-OBz-Y**; Y = OMe, Me, H, Cl, COMe, CN, or $NO_2$) with a slope value of $\rho = 0.568$ (plot constructed comparing yields of **3a** obtained at 3 h from **4a-OBz-Y** *versus* **4a-OBz-H**). (b) Nucleofugality Brønsted plot ($R^2 = 0.966$) of **4a-OBz-Y** (Y = OMe, Me, H, Cl, COMe, CN, $NO_2$) complexes with a slope value of $\beta_{LG} = -0.573$. (c) Linear correlation ($R^2 = 0.973$) between the $^{13}C$ chemical shift of C2 and Hammett parameters of **4a-OBz-Y** (Y = OMe, Me, H, Cl, COMe, CN, or $NO_2$) complexes. (d) Linear correlation ($R^2 = 0.949$) between Gibbs energy barriers of the $S_N2$-type transition state ($\Delta G^{\ddagger}(S_N2)$, full details can be found in Table S9 and Fig. S20†) and Hammett parameters of **4a-OBz-Y** (Y = OMe, Me, H, Cl, COMe, CN, or $NO_2$) complexes; yields calculated by $^1H$ NMR analysis using 1,3,5-trimethoxybenzene as the internal standard.

electron density on C2, subsequently modifying its electrophilic character. Thus, when EWGs are attached to the benzoate moiety, C2 becomes more electrophilic and subsequently more reactive towards a substitution. This trend was also observed when the theoretical activation barriers of the different *para*-substituted benzoate **4a-OBz-Y** complexes were compared with Hammett $\sigma_p$ (Gibbs energies were used for the linear correlation *vs.* Hammett parameters; see the ESI† for full details). The plot in Fig. 2d shows that **4a-OBz-NO$_2$** has a lower activation barrier ($\Delta G^{\ddagger} = 30.0$ kcal mol$^{-1}$) compared to the electron-rich **4a-OBz-OMe** ($\Delta G^{\ddagger} = 27.3$ kcal mol$^{-1}$) species and the trend observed ($R^2 = 0.949$) is in agreement with the experimental linear correlations mentioned above. Further evidence for an $S_N2$-type event was obtained by evaluating the impact of the nucleophile strength on the activation barrier, *i.e.* by computing different *p*-aryl substitutions on the ligand backbone (Fig. 3 and S30†). Starting from the electron-rich **4b-OAc** (R = *p*-OMe) complex, the $S_N2$-type barrier decreases by around 2 kcal mol$^{-1}$ (**TS3b**; 27.0 kcal mol$^{-1}$) compared to the previously reported activation energy starting from **4a-OAc** (**TS3a**; 28.9 kcal mol$^{-1}$).[61] Contrariwise, when the $S_N2$-type barrier is calculated for a poorer nucleophilic aryl-Co(III) complex such as **4c-OAc** (R = *p*-NO$_2$), a substantial increase can be observed (**TS3c**; 34.7 kcal mol$^{-1}$). Thus, these theoretical studies suggest that the nucleophilic character of the aryl-Co(III) bond plays a key role in the C–C bond forming/C–O cleavage event.

All these results taken together indicate a transition state in the rate-determining step which builds partial negative charge ($\rho > 0$), depends on the *para*-substituents of the benzoate moiety and presents a considerable sensitivity to both the leaving group ability ($\beta_{LG} < 0$) and the nucleophilicity of the aryl-Co(III) moiety (Fig. 3). Indeed, these results strongly suggest a plausible transition state in which a simultaneous C–C bond formation/C–O cleavage event is occurring in a concerted intramolecular $S_N2$-type reaction.

Further experimental evidence of a unique $S_N2$-type intramolecular mechanism was obtained when *para*-substituted **4a-OBz-Y** were studied by high-resolution mass spectrometry (HRMS) (Fig. 4). Indeed, the corresponding organometallic product of an intramolecular substitution (**INT-MI′**) was detected when MS/MS analysis was performed for the mass peak corresponding to **4a-OBz-Y**, irrespective of the nature of substituent Y (Y = OMe, Me, H, Cl, COMe, CN, or NO$_2$). A single peak which corresponds to a fragment involving the loss of the corresponding carboxylic acid ([**INT-MI**-RCOOH]$^+$ = $C_{19}H_{21}CoN_3O_2^+$; simulated *m*/*z* = 382.0960; Fig. 4) was observed regardless of the carboxylate moiety present in the isolated compounds, which suggests the same product for each **4a-OBz-Y** species. Furthermore, the relative intensity of **INT-MI′** at the same collision energy (15 eV, see also Fig. S6–S13†) is higher when an electron-poor *p*-substituted benzoate is present in **4a-OBz-Y** (rel. intensity of 55.6% and 65.3% when Y = NO$_2$ and CN, respectively) compared to electron-rich substituents (rel. intensity of 10.9% and 14.8% when Y = OMe and Me, respectively). This trend strongly supports the nucleofugality trend of the *para*-substituted leaving groups (Fig. 2b) as well as the electrophilic character of C2 (Fig. 2c), indicating that with electron-poor benzoates the C–C bond formation/C–O bond cleavage event is easier and subsequently faster.

At this point our interest was focused on the reaction of α-substituted diazoacetates, particularly on the reaction of **2a-OAc** with electron-rich (**i**) and electron-poor (**l**) carbene precursors. As shown in Scheme 5b, the reaction of α-phenyl diazoacetates is slower when compared to that of ethyl diazoacetate, which suggests steric influence or even other reaction pathways not considered before. Furthermore, it has been shown that electron-rich diazoacetates do not inhibit the reaction with other carbene precursors (Scheme 5c). Thus, **2a-OAc** was reacted with 2.0 equiv. of diazoacetates **i** and **l** over 60 min (Scheme 7), and the reaction crudes were analyzed by HRMS. With electron-rich diazoacetate **i**, the corresponding organometallic **4a-OAc-PhOMe** intermediate was not detected in agreement with the reactivity observed in Scheme 4 (see Fig. S14†). In contrast, when electron-poor diazoacetate **l** was reacted with **2a-OAc**, a peak at *m*/*z* = 563.1335 corresponding to **4a-OAc-PhNO$_2$** was observed ($C_{27}H_{28}N_4O_6Co^+$; simulated *m*/*z* = 563.1335, Fig. S15†) indicating the formation of a similar C-metalated aryl-Co(III) enolate which can be considered either as a carbenoid or a masked-carbene. Further evidence of the formation of this particular cobaltacycle was found when MS/MS analysis of the 563.1335 peak for **4a-OAc-PhNO$_2$** was performed. A single peak with *m*/*z* = 503.1128 was observed (20 eV), which corresponds to a fragment involving the loss of acetic acid ($C_{25}H_{24}N_4O_4Co^+$, simulated *m*/*z* = 503.1124; Fig. S16†), similarly to when MS/MS analysis was applied to *para*-substituted **4a-OBz-Y** species in Fig. 4. Indeed, this species corresponds to the previously observed analogous **INT-MI′** with EDA derivatives, thus indicating the formation of a C-metalated aryl-Co(III) enolate when α-phenyl diazoacetates are utilized as coupling partners.

The effect of several additives on the $S_N2$-type pathway was also evaluated (see Scheme 8). It has been proven both experimentally and theoretically that Lewis acids assist the C–C bond formation/C–O cleavage event and accelerate the reaction, particularly in the case of LiOTf.[61] Furthermore, recent studies demonstrate that Lewis acids have beneficial effects on C–H

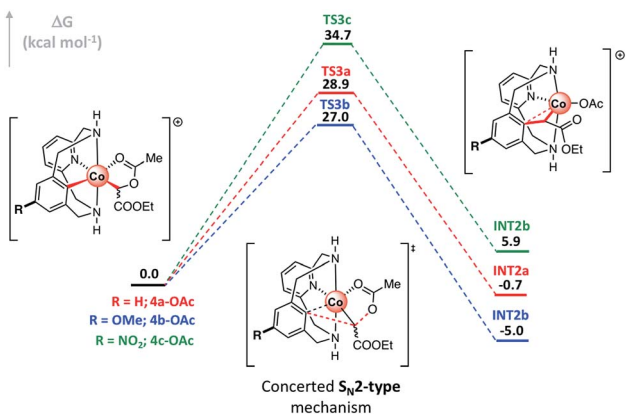


Fig. 3 Gibbs energy profile of the $S_N2$-type event of *p*-substituted C-metalated aryl-Co(III) complex enolates **4x-OAc** (R = H (x = **a**), OMe (x = **b**) and NO$_2$ (x = **c**)). Relative Gibbs energy values are given in kcal mol$^{-1}$ (see Fig. S30† for full profiles).

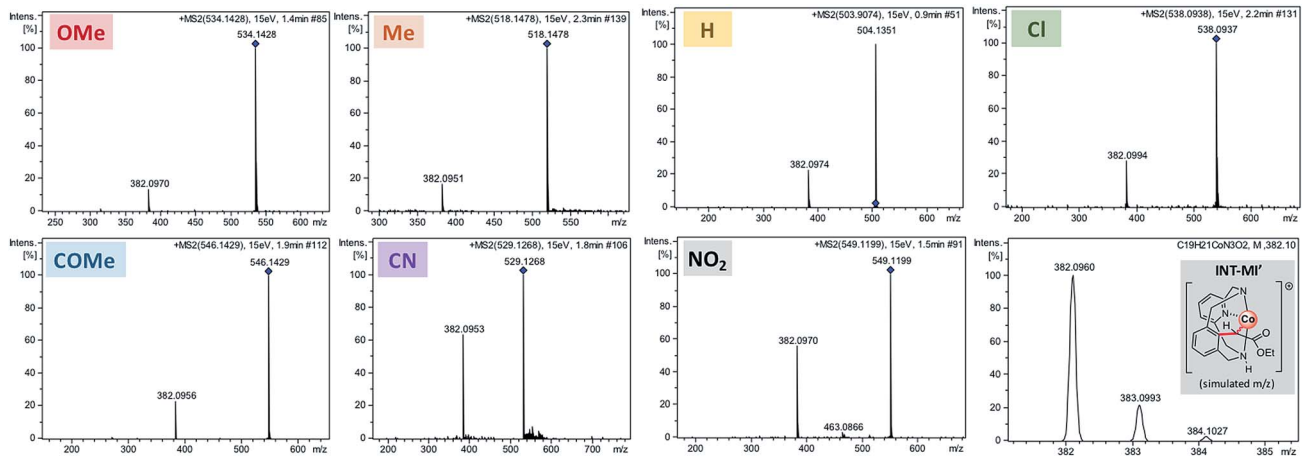


Fig. 4 Detection of **INT-MI'** (simulated $m/z$ = 382.0960) by MS/MS studies of organometallic **4a-OBz-Y** complexes: **4a-OBz-OMe** ($m/z$ = 534.1428), **4a-OBz-Me** ($m/z$ = 518.1478), **4a-OBz** ($m/z$ = 504.1351), **4a-OBz-Cl** ($m/z$ = 538.0949), **4a-OBz-COMe** ($m/z$ = 546.1429), **4a-OBz-CN** ($m/z$ = 529.1268) and **4a-OBz-NO$_2$** ($m/z$ = 538.0949).

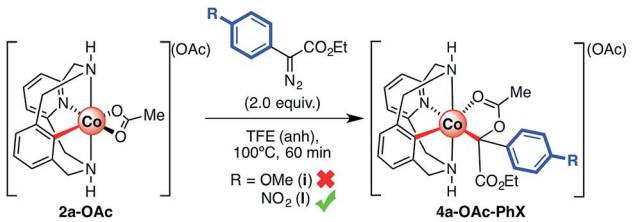


Scheme 7 Reaction of **2a-OAc** with α-substituted ethyldiazoacetates and HRMS analysis of reaction crudes.

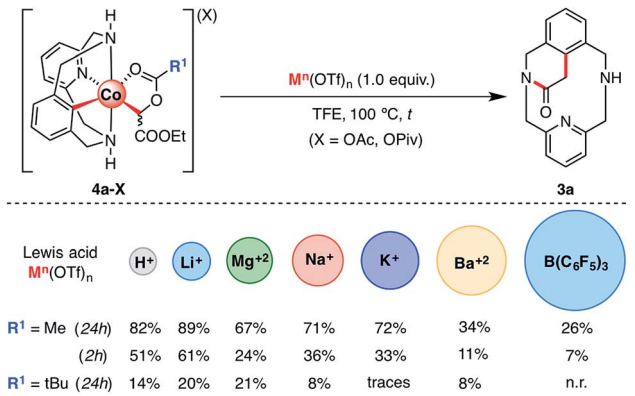


Scheme 8 Evolution of organometallic **4a-X** (X = **OAc** and **OPiv**) intermediates to **3a** in the presence of several Lewis acids as additives (see Scheme S14 and Table S6† for details).

activation methodologies using Co(III) as a catalyst, both assisting C–H activation and carbene formation.[46] Based on these pioneering studies, we explored the possibility of adding other similar Lewis acids such as MOTf (M = H, Li, Na, or K), M(OTf)$_2$ (M = Mg or Ba) and other larger but highly acidic compounds such as tris(pentafluorophenyl)borane (Scheme 8). Thus, **4a-OAc** was mixed with 1.0 equiv. of Lewis acid at 100 °C. After 24 h, good to excellent yields of **3a** were obtained with organic acids such as HOTf (82%) and metal cations such as LiOTf (89%), Mg(OTf)$_2$ (67%), NaOTf (71%) and KOTf (72%). Interestingly, a poor yield (34%) was obtained when Ba(OTf)$_2$ was used as an additive. Finally, with boron-based Lewis acids such as B(C$_6$F$_5$)$_3$, **3a** was observed only in 26% yield. This latter result suggests that the evolution of **4a-OAc** to **3a** depends both on Lewis acid strength and bulkiness.

In order to gain more information about the effects of the different additives used to promote the evolution of **4a-OAc** to **3a**, the same reaction was run over a shorter time period. After 2 h, **3a** was obtained in good yields using acids such as LiOTf (61%) and HOTf (51%). However, a moderate-to-poor yield of **3a** was obtained when larger and less acidic metal cations such as NaOTf (36%), KOTf (33%), Mg(OTf)$_2$ (24%) and Ba(OTf)$_2$ (11%) were added. In addition, following the reactivity trend observed after 24 h, a low yield (7%) of **3a** was obtained when tris(pentafluorophenyl)borane was added, which suggests that large Lewis acids hinder the interaction between the Lewis acid and the organometallic **4a-OAc** complex, hence preventing its activation towards an intramolecular S$_N$2-type reaction. Indeed, similar results were obtained when **4a-OPiv** was subjected to the same reaction conditions. In this case, however, poor yields were obtained even with hard Lewis acids such as LiOTf (20%) or HOTf (14%) and the reaction was completely inhibited with larger Lewis acids such as KOTf, Ba(OTf)$_2$ or B(C$_6$F$_5$)$_3$. Indeed, steric hindrance is a plausible reason for the lack of reactivity of **2a-TPA** with EDA even in the presence of additives such as LiOTf or H$_2$O (see Scheme 3 for further details).

To gain further insight into the interaction of different Lewis acids (LA) with **4a-OAc** we performed computational studies focused on the intramolecular LA-assisted S$_N$2-type event (see the ESI† for computational details). To do so, we considered the explicit inclusion of cationic metal ions M$^+$ (M = Li, Na, and K) in the computational analysis of the C–C bond formation/C–O cleavage event. In order to properly determine the Gibbs energy of **4a-OAc-M(TFE)$_3$** adduct formation taking into account the solvent environment of the alkali cations, at least three explicit

TFE molecules had to be included in the DFT calculations (Fig. 5 and S23†). This event is exergonic for the three alkali metals.

In agreement with experimental results, the activation barrier for the $S_N2$-type C–C bond formation/C–O cleavage event decreases compared to the same step in the absence of additives ($\Delta G^{\ddagger} = 28.9$ kcal mol$^{-1}$, see Fig. 3).[61] Interestingly, a clear trend in agreement with the reactivity observed in Scheme 6 was found (Fig. 6). In fact, the increase of the activation energy of the LA-assisted $S_N2$ step correlates with the size and strength of the corresponding Lewis acid: $\Delta G^{\ddagger}(Li^+) = 22.6 < \Delta G^{\ddagger}(Na^+) = 24.7 < \Delta G^{\ddagger}(K^+) = 25.2$ kcal mol$^{-1}$. Thus, when Lewis acids are added to the reaction media, they coordinate to **4a-OAc** (O2 and O3, Fig. 1), turning the carboxylate moiety into a better leaving group through a LA-mediated carboxylate activation. However, as calculations show in Fig. 6 and reactivity studies suggest (Scheme 8), the carboxylate activation depends on both the strength of the Lewis acid and its size.

The mechanism of the corresponding C–C bond formation and C–O bond cleavage event for the electron-poor $\alpha$-*p*-$NO_2$-phenyl diazoacetate (**l**) was further studied by means of DFT calculations (for full details see the ESI†). The reaction profile in Fig. 7 shows that **2a-OAc** reacts with diazoacetate **l** to form an adduct (**Adduct**, $\Delta G = 11.8$ kcal mol$^{-1}$) in which the acetate ligand is coordinated in a monodentate fashion. Then, the adduct with the corresponding diazoacetate evolves to **4a-OAc-PhNO$_2$** ($\Delta G = -26.9$ kcal mol$^{-1}$) through an activation barrier of $\Delta G^{\ddagger} = 28.4$ kcal mol$^{-1}$ (**TS1**) in a highly exergonic process. Interestingly, the formation of a transient carbene species was not observed computationally and **4a-OAc-PhNO$_2$** was directly obtained from the adduct with diazoacetate **l**. As mentioned before, experimental evidence of the formation of **4a-OAc-PhNO$_2$** species was also obtained by HRMS studies (Fig. 4), which agrees with the DFT calculations presented in Fig. 7. Then, **4a-OAc-PhNO$_2$** could evolve to **INT-MI-PhNO$_2$** ($\Delta G = -9.3$ kcal mol$^{-1}$) through a highly asynchronous late transition state (**TS2**, $\Delta G = 9.9$ kcal mol$^{-1}$; see Fig. 8, right). Interestingly, **TS2** is strongly asynchronous, contrariwise to the corresponding TS for **4a-OAc** (Fig. 8, left) which shows a clearly

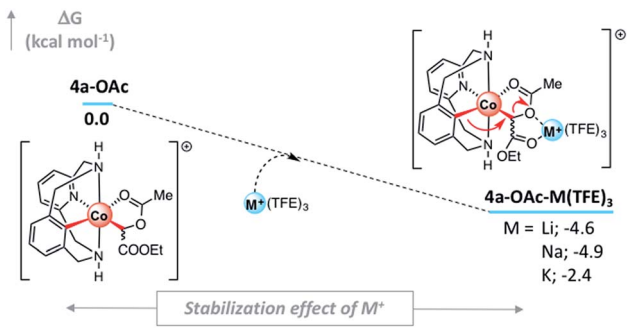


Fig. 5 (a) DFT Gibbs energy of the adduct formation when **4a-OAc** is mixed with $M^+$ cationic Lewis acids (M = Li, Na and K) taking into account the presence of three explicit TFE molecules. Relative Gibbs energy values are given in kcal mol$^{-1}$; concentration of the solvated $M^+ = 0.039$ mol L$^{-1}$ (see Fig. S22–S24† for details).

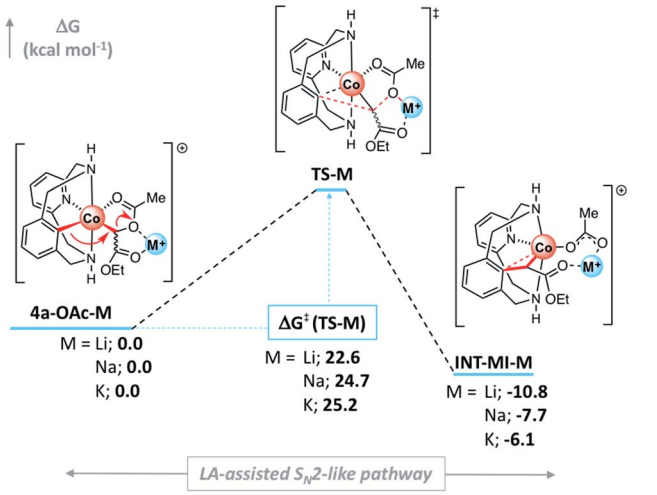


Fig. 6 Gibbs energy profile of the $S_N2$-type event in the presence of several $M^+$ cationic Lewis acids (M = Li, Na and K). Relative Gibbs energy values are given in kcal mol$^{-1}$ (see Fig. S21† for details).

synchronous transition state. Thus, although the $S_N2$-event occurs in a concerted manner for both **4a-OAc** and **4a-OAc-PhNO$_2$**, the IRC calculation connecting **4a-OAc-PhNO$_2$**, **TS2** and **INT-MI-PhNO$_2$** (see Fig. S27†) shows a first C–O bond breaking followed by the formation of the C–C bond, the latter determining the Gibbs energy and geometry of **TS2**. The high activation barrier of this process ($\Delta G^{\ddagger} = 36.8$ kcal mol$^{-1}$) hampers this transformation, which agrees with the experimental results obtained when **2a-OAc** reacts with diazoacetate **l** in the absence of additives (Table S2,† entry 13). Despite the highly energetic

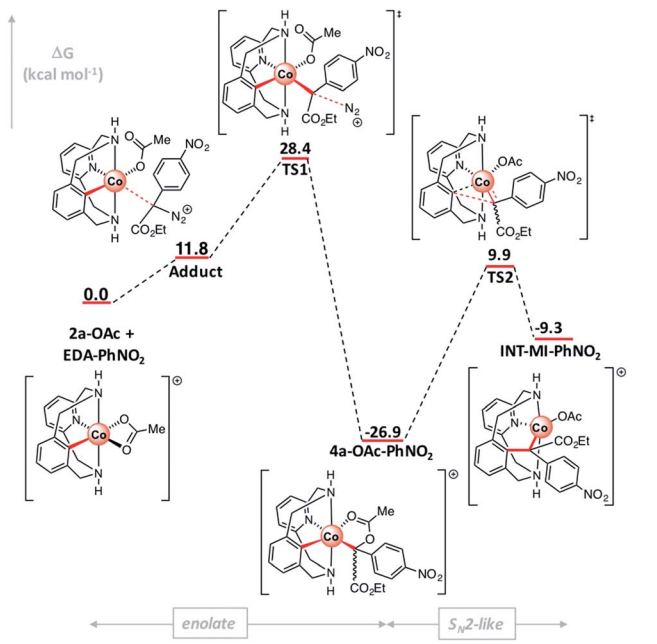


Fig. 7 Gibbs energy profile of C-metalated aryl-Co(III) enolate formation and the $S_N2$-type event using diazoacetate **l**. Relative Gibbs energy values are given in kcal mol$^{-1}$ (see Fig. S26† for details).

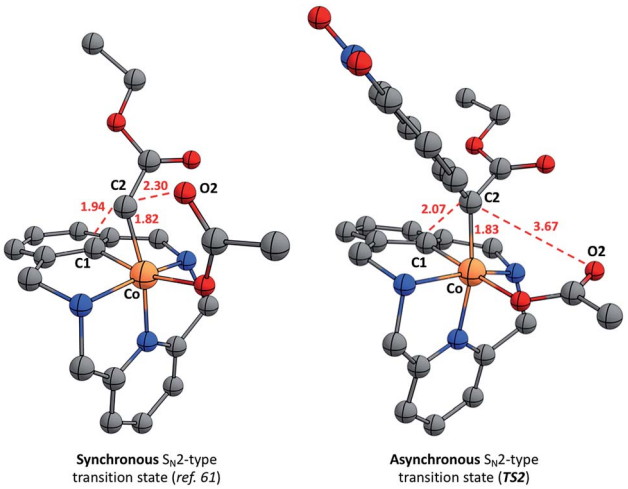


Fig. 8 Computed transition state structures of the corresponding concerted $S_N2$-type C–C bond forming step with ethyl diazoacetate (left, synchronous) and diazoacetate **l** (right, asynchronous). Selected bond distances are depicted in red (Å).

transition state (**TS2**) and the endergonic process from **4a-OAc-NO$_2$** to **INT-MI-NO$_2$**, the latter species could be detected by HRMS when MS/MS analysis was applied to **4a-OAc-NO$_2$** with a high collision energy (20 eV). Thus, the need for a high collision energy in MS/MS analysis agrees with the theoretical results depicted in Fig. 7.

Experimental results clearly indicate that in the presence of 1.0 equiv. of Li(OTf) the reaction proceeded with excellent yields while in its absence poor yields were obtained (see Scheme 4, **3l**). Thus, we considered the explicit inclusion of a lithium cation in the computational analysis of the C–O cleavage/C–C bond formation event (Fig. 9). Again, the interaction of the solvated $Li^+$ with the complex is exergonic ($\Delta G$ = −2.4 kcal mol$^{-1}$, see Fig. S29†).

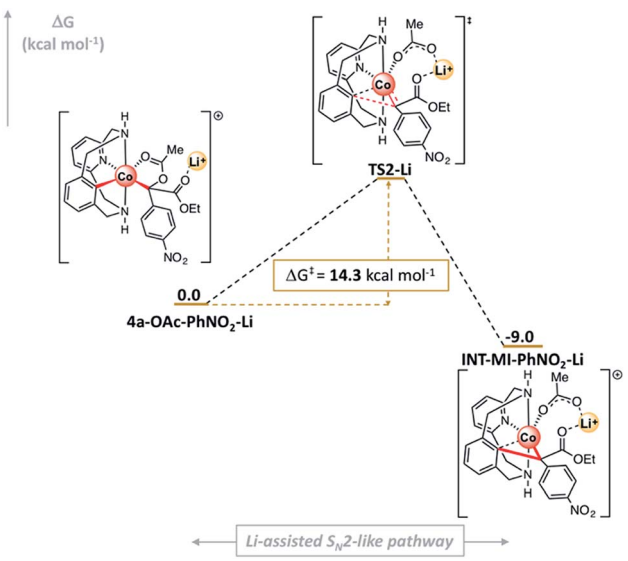


Fig. 9 Gibbs energy profile of the $S_N2$-type event using diazoacetate **l** in the presence of $Li^+$. Relative Gibbs energy values are given in kcal mol$^{-1}$ (see Fig. S28† for details).

Then, **4a-OAc-PhNO$_2$-Li** evolves to **INT-MI-NO$_2$-Li** ($\Delta G$ = −9.0 kcal mol$^{-1}$; Fig. 9) overcoming a barrier of 14.3 kcal mol$^{-1}$ in an asynchronous exergonic process. Again, the C–O bond cleavage is followed by the C–C bond formation, which determines the structure of **TS2-Li**. Strikingly, when a $Li^+$ ion interacts with the organometallic **4a-OAc-NO$_2$** complex, the activation barrier for the $S_N2$-like pathway decreases by 22.5 kcal mol$^{-1}$ ($\Delta\Delta G^{\ddagger}$ = 36.8 (**TS2**, Fig. 7) – 14.3 (**TS2-Li**, Fig. 9) kcal mol$^{-1}$). Thus, when Lewis acids are added to the reaction media, they coordinate to the ester and carboxylate moieties in **4a-OAc-PhNO$_2$**, turning the latter into better leaving groups through a LA-mediated carboxylate activation and subsequently favoring the formation of the cyclic amide product **3l**.

It should be noted that the $S_N2$-type event occurs in an electrophilic tertiary carbon in an asynchronous manner, which constitutes a rare example of bimolecular substitution reaction. Subsequently, after the unprecedented Co(III)-mediated intramolecular $S_N2$-type C–C bond formation, **INT-MI-PhNO$_2$** evolves to **3** through a protodemetalation step and a subsequent LA-assisted cyclization (Scheme 2), as reported in previously reported Co(III)-catalyzed diazoacetate coupling protocols.[47,48,51,61]

After studying the effect of Lewis acids on the formation of cyclic amides **3**, we turned our attention to the final cobalt species generated after reaction completion. In previous studies, organometallic **2a-OAc** and **4a-OAc** were successfully applied as catalysts for the functionalization of **1a-H** with EDA under an inert atmosphere, which excludes reaction pathways that imply oxidation state changes.[61] To obtain further evidence of a plausible redox-neutral reactivity, XAS spectroscopy was applied to determine the oxidation state of cobalt at the end of the reaction, as well as its possible coordination environment (Scheme 9). The XAS spectrum of the final reaction crude shows a rising edge at 7720 eV with a pre-edge centered at 7710.5, consistent with that of previously reported Co(III) species from our group.[60,61] These XAS features suggest that the final cobalt species is a Co(III) compound, indicating a redox neutral mechanism in which cobalt does not change its oxidation state. Indeed, this redox-neutral mechanism was previously proposed in similar transformations with Cp*Co(III) catalysts.[46–51]

Further EXAFS analysis (Scheme 9b, right) shows a first coordination sphere consisting of two shells of scattering atoms with two/three N/O atoms in the 2.00–2.04 Å range and three/four N/O atoms in the 2.14–2.18 Å range. Furthermore, taking into account that scattering paths from possible acetate ligands bound in a bidentate fashion significantly improve the fit, the presence of two acetate ligands coordinating the Co(III) centre is plausible (see Table S7†). The shorter scattering shell is consistent with what might be expected for a Co(III) coordination sphere; however, the longer scattering shell suggests some decomposition of Co(III) to Co(II) due to the previously reported reductant effect of ethyl diazoacetate.[65] Indeed, Co(II) acetate has a pre-edge centered at ~7709.5 eV,[66] similar to the 7709.7 eV fitted pre-edge peak in Scheme 9. Thus, the obtained XANES analysis results, together with previously reported examples,[45–50,60] suggest a redox-neutral mechanism in which Co(III) does not change its oxidation state.

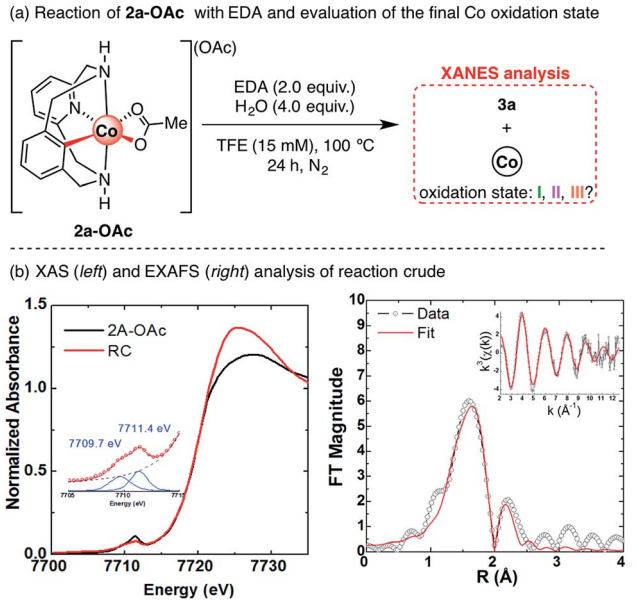


Scheme 9 (a) Evolution of **4a-OAc** to **3a** and (b) XAS of the crude reaction mixture. Left: XANES region showing the rising edge of final "$Co^{+n}$" species overlaid with the **2a-OAc** spectrum previously reported; inset: fitted pre-edge of final "$Co^{+n}$" species. Right: Fourier-transformed EXAFS spectra of final "$Co^{+n}$" species; inset: $k^3$-weighted unfiltered EXAFS spectra.

## Conclusions

In summary, a family of C-metalated aryl-Co(III) enolates or masked-carbenes has been synthesized using diazoacetates and they have been characterized through several techniques including XRD. The scope of diazoacetates has been evaluated, showing a clear preference for electron-poor carbene precursors to furnish the corresponding macrocyclic amide products through a proposed $S_N2$-type pathway. Indeed, exhaustive experimental and theoretical studies indicate that an intramolecular $S_N2$-type process occurs from **4a-X** complexes, which are necessary intermediates to deliver the alkyl fragment to construct the new C–C bond. Further studies with α-substituted diazoesters also suggest an unprecedented intramolecular asynchronous $S_N2$-type pathway occurring in tertiary carbons. Furthermore, the experimental key role of Lewis acids is reflected in theoretical studies, unveiling a LA-carboxylate-activation event that considerably favours the C–O bond cleavage/C–C bond formation. The profound mechanistic understanding of this carboxylate-assisted taming of otherwise metastable carbenes is expected to become a new tool in the design of novel carbene-based metal-catalyzed C–C transformations.

## Conflicts of interest

There are no conflicts to declare.

## Acknowledgements

We acknowledge financial support from the European Research Council for the Starting Grant Project ERC-2011-StG-277801 to X. R. and from MINECO of Spain for project CTQ2016-77989-P to A. C. and X. R. and project CTQ2014-52525-P to J. M. L. We also thank the Generalitat de Catalunya for projects 2017SGR264 and 2014SGR931. We thank the MECD and MINECO of Spain for a FPU grant to O. P. and a FPI grant to S. R. X. R. also thanks ICREA for an ICREA Acadèmia award, and COST CHAOS (CA15106). We acknowledge SOLEIL for provision of synchrotron radiation facilities and we would like to thank Dr Landrot Gautier for assistance in using beamline SAMBA. We also thank Dr Laura Gómez (HRMS) and Xavier Fontrodona (XRD) from Serveis Tècnics de Recerca of the Universitat de Girona.

## Notes and references

1 T. Newhouse and P. S. Baran, *Angew. Chem., Int. Ed.*, 2011, **50**, 3362–3374.
2 L. McMurray, F. O'Hara and M. J. Gaunt, *Chem. Soc. Rev.*, 2011, **40**, 1885–1898.
3 P. Thansandote and M. Lautens, *Chem.–Eur. J.*, 2009, **15**, 5874–5883.
4 G. Song, F. Wang and X. Li, *Chem. Soc. Rev.*, 2012, **41**, 3651.
5 T. Satoh and M. Miura, *Chem.–Eur. J.*, 2010, **16**, 11212–11222.
6 X. Chen, K. M. Engle, D.-H. Wang and J.-Q. Yu, *Angew. Chem., Int. Ed.*, 2009, **48**, 5094–5115.
7 S. Enthaler and A. Company, *Chem. Soc. Rev.*, 2011, **40**, 4912–4924.
8 L. Ackermann, *Modern Arylation Methods*, Wiley-VCH Verlag GmbH & Co. KGaA, Weinheim, Germany, 2009.
9 L. Ackermann, *Acc. Chem. Res.*, 2014, **47**, 281–295.
10 L. Wang and L. Ackermann, *Chem. Commun.*, 2014, **50**, 1083–1085.
11 J. Miao and H. Ge, *Eur. J. Org Chem.*, 2015, **2015**, 7859–7868.
12 G. Pototschnig, N. Maulide and M. Schnürch, *Chem.–Eur. J.*, 2017, **23**, 9206–9232.
13 B. Su, Z.-C. Cao and Z.-J. Shi, *Acc. Chem. Res.*, 2015, **48**, 886–896.
14 J. E. Zweig, D. E. Kim and T. R. Newhouse, *Chem. Rev.*, 2017, **117**, 11680–11752.
15 L. Ilies and E. Nakamura, in *C-H Bond Activation and Catalytic Functionalization II*, ed. P. H. Dixneuf and H. Doucet, Springer International Publishing, Cham, 2016, pp. 1–18.
16 M. Su, C. Li and J. Ma, *J. Chin. Chem. Soc.*, 2016, **63**, 828–840.
17 R. Shang, L. Ilies and E. Nakamura, *Chem. Rev.*, 2017, **117**, 9086–9139.
18 W. Liu and L. Ackermann, *ACS Catal.*, 2016, **6**, 3743–3752.
19 W. Liu and J. T. Groves, *Acc. Chem. Res.*, 2015, **48**, 1727–1735.
20 J. Yamaguchi, K. Muto and K. Itami, *Top. Curr. Chem.*, 2016, 374.
21 R. Becker and W. D. Jones, in *Catalysis without Precious Metals*, Wiley-VCH Verlag GmbH & Co. KGaA, Weinheim, Germany, 2010, pp. 143–164.
22 K. Gao and N. Yoshikai, *Acc. Chem. Res.*, 2014, **47**, 1208–1219.
23 M. Moselage, J. Li and L. Ackermann, *ACS Catal.*, 2016, **6**, 498–525.
24 D. Wei, X. Zhu, J.-L. Niu and M.-P. Song, *ChemCatChem*, 2016, **8**, 1242–1263.

25 P. G. Chirila and C. J. Whiteoak, *Dalton Trans.*, 2017, **46**, 9721–9739.
26 S. Wang, S.-Y. Chen and X.-Q. Yu, *Chem. Commun.*, 2017, **53**, 3165–3180.
27 T. Yoshino and S. Matsunaga, *Adv. Synth. Catal.*, 2017, **359**, 1245–1262.
28 Y. Kommagalla and N. Chatani, *Coord. Chem. Rev.*, 2017, **350**, 117–135.
29 O. Planas, P. G. Chirila, C. J. Whiteoak and X. Ribas, *Adv. Organomet. Chem.*, 2018, **69**, 209–282.
30 S. Maity, R. Kancherla, U. Dhawa, E. Hoque, S. Pimparkar and D. Maiti, *ACS Catal.*, 2016, **6**, 5493–5499.
31 X. Yu, K. Chen, S. Guo, P. Shi, C. Song and J. Zhu, *Org. Lett.*, 2017, **19**, 5348–5351.
32 K. Kanamori, W. E. Broderick, R. F. Jordan, R. D. Willett and J. I. Legg, *J. Am. Chem. Soc.*, 1986, **108**, 7122–7124.
33 W. E. Broderick, K. Kanamori, R. D. Willett and J. I. Legg, *Inorg. Chem.*, 1991, **30**, 3875–3881.
34 T. Avilés, A. Dinis, M. J. Calhorda, P. Pinto, V. Félix and M. G. B. Drew, *J. Organomet. Chem.*, 2001, **625**, 186–194.
35 L. Grigorjeva and O. Daugulis, *Angew. Chem., Int. Ed.*, 2014, **53**, 10209–10212.
36 Y. Baek, S. Kim, B. Jeon and P. H. Lee, *Org. Lett.*, 2016, **18**, 104–107.
37 K. Ramakrishna and C. Sivasankar, *Eur. J. Org. Chem.*, 2017, **2017**, 4035–4043.
38 B. G. Das, A. Chirila, M. Tromp, J. N. H. Reek and B. de Bruin, *J. Am. Chem. Soc.*, 2016, **138**, 8968–8975.
39 Y. Wang, X. Wen, X. Cui, L. Wojtas and X. P. Zhang, *J. Am. Chem. Soc.*, 2017, **139**, 1049–1052.
40 T. Ikeno, I. Iwakura and T. Yamada, *J. Am. Chem. Soc.*, 2002, **124**, 15152–15153.
41 H. Lu, W. I. Dzik, X. Xu, L. Wojtas, B. de Bruin and X. P. Zhang, *J. Am. Chem. Soc.*, 2011, **133**, 8518–8521.
42 S. Roy, S. K. Das and B. Chattopadhyay, *Angew. Chem., Int. Ed.*, 2018, **57**, 2238–2243.
43 C. te Grotenhuis, N. van den Heuvel, J. I. van der Vlugt and B. de Bruin, *Angew. Chem., Int. Ed.*, 2018, **57**, 140–145.
44 C. te Grotenhuis, B. G. Das, P. F. Kuijpers, W. Hageman, M. Trouwborst and B. de Bruin, *Chem. Sci.*, 2017, **8**, 8221–8230.
45 T. Yao, K. Hirano, T. Satoh and M. Miura, *Angew. Chem., Int. Ed.*, 2012, **51**, 775–779.
46 J. H. Kim, S. Greßies and F. Glorius, *Angew. Chem., Int. Ed.*, 2016, **55**, 5577–5581.
47 D. Zhao, J. H. Kim, L. Stegemann, C. A. Strassert and F. Glorius, *Angew. Chem., Int. Ed.*, 2015, **54**, 4508–4511.
48 J. Li, M. Tang, L. Zang, X. Zhang, Z. Zhang and L. Ackermann, *Org. Lett.*, 2016, **18**, 2742–2745.
49 S.-Y. Yan, P.-X. Ling and B.-F. Shi, *Adv. Synth. Catal.*, 2017, **359**, 2912–2917.
50 X.-G. Liu, S.-S. Zhang, J.-Q. Wu, Q. Li and H. Wang, *Tetrahedron Lett.*, 2015, **56**, 4093–4095.
51 S. Qu and C. J. Cramer, *J. Org. Chem.*, 2017, **82**, 1195–1204.
52 F. Hu, Y. Xia, C. Ma, Y. Zhang and J. Wang, *Chem. Commun.*, 2015, **51**, 7986–7995.
53 M. Font, F. Acuña-Parés, T. Parella, J. Serra, J. M. Luis, J. Lloret-Fillol, M. Costas and X. Ribas, *Nat. Commun.*, 2014, **5**, 4373.
54 A. Casitas, M. Canta, M. Solà, M. Costas and X. Ribas, *J. Am. Chem. Soc.*, 2011, **133**, 19386–19392.
55 A. Casitas, A. E. King, T. Parella, M. Costas, S. S. Stahl and X. Ribas, *Chem. Sci.*, 2010, **1**, 326.
56 M. Rovira, S. Roldán-Gómez, V. Martin-Diaconescu, C. J. Whiteoak, A. Company, J. M. Luis and X. Ribas, *Chem.–Eur. J.*, 2017, **23**, 11662–11668.
57 X. Ribas and M. Devillard, *Chem.–Eur. J.*, 2018, **24**, 1222–1230.
58 W. Zhou, S. Zheng, J. W. Schultz, N. P. Rath and L. M. Mirica, *J. Am. Chem. Soc.*, 2016, **138**, 5777–5780.
59 W. Zhou, J. W. Schultz, N. P. Rath and L. M. Mirica, *J. Am. Chem. Soc.*, 2015, **137**, 7604–7607.
60 O. Planas, C. J. Whiteoak, V. Martin-Diaconescu, I. Gamba, J. M. Luis, T. Parella, A. Company and X. Ribas, *J. Am. Chem. Soc.*, 2016, **138**, 14388–14397.
61 O. Planas, S. Roldán-Gómez, V. Martin-Diaconescu, T. Parella, J. M. Luis, A. Company and X. Ribas, *J. Am. Chem. Soc.*, 2017, **139**, 14649–14655.
62 Y. Aihara and N. Chatani, *Chem. Sci.*, 2013, **4**, 664–670.
63 A. Yokota, Y. Aihara and N. Chatani, *J. Org. Chem.*, 2014, **79**, 11922–11932.
64 E. V. Anslyn and D. A. Dougherty, *Modern Physical Organic Chemistry*, 2006, vol. 69.
65 J. R. Wolf, C. G. Hamaker, J.-P. Djukic, T. Kodadek and L. K. Woo, *J. Am. Chem. Soc.*, 1995, **117**, 9194–9199.
66 M. Mrak, N. N. Tušar, A. Ristić, I. Arčon, F. Thibault-Starzyk and V. Kaučič, *Microporous Mesoporous Mater.*, 2002, **56**, 257–266.